Austenite Formation Kinetics During Rapid Heating in a Microalloyed Steel

J. D. Puskar[†], R. C. Dykhuizen[†], C. V. Robino[†], M. E. Burnett[‡], J. B. Kelley[†]

[†]Sandia National Laboratories
Albuquerque, NM 87185

[‡]The Timken Company
Canton, OH 44706

Key Words: Austenite, Microalloy, On Heating Kinetics, Model, Gleeble, Dilatometry

INTRODUCTION

The formation of austenite at rapid heating rates is an important aspect of many metallurgical processing and fabricating schemes for steels. For example, hot working, heat treating, and welding all require or result in heating into the austenite or austenite plus ferrite phase fields. At the present time, there is widespread interest in modeling these processes as an aid in optimization and control of post-process microstructure, properties and distortion. Additionally, these models will enable steel producers to identify optimized compositions and microstructures for various classes of applications. For these models to be applicable, they must describe the phase transformation kinetics associated with both the on-heating and on-cooling transformations, and these descriptions must be experimentally validated. In general, the formation of austenite in steels has received less attention than the decomposition of austenite, although there have been a number of experimental[1-6] and numerical studies[7-12] of the process. These studies have yielded significant insight into the transformation from both mechanistic and computational perspectives, but there are some limitations and difficulties in applying this insight to large scale process modeling.

As discussed by Gavard *et al.*[13], and Akbay *et al.*[9] the formation of austenite differs from its decomposition in two principal ways. First, in the case of diffusion-limited on-cooling transformations, the driving force for the reaction increases with increasing undercooling below the equilibrium transformation temperature, while diffusion rates decrease with increasing undercooling. The balance between driving force and diffusion rates results in the classical C-curve kinetic behavior, in which the overall transformation rate experiences a maximum at intermediate undercoolings. In contrast, for the on-heating transformation, both the driving force and diffusion rates increase with temperature above the equilibrium transformation temperature, so that the rate of transformation continuously increases with temperature. Also, for the on-cooling reactions from homogeneous austenite, the kinetics can be fully described in terms of the composition and austenite grain size. However, such a simplification is not possible for the formation of austenite since a wide variety of starting microstructures are possible.

Recently, a numerical model was developed to describe the formation of austenite in pearlitic hypoeutectoid plain carbon steels.[14] The model extracts the austenite formation kinetics directly from dilatation data for continuous heating experiments. A low carbon steel, 1026, was used to develop and validate the model which is based on a two step description of the process. The first step utilizes a classical description of the decomposition of the pearlite constituent, while the second step uses a one-dimensional diffusion model to describe the growth of the austenite into the proeutectoid ferrite.

Microalloyed steels are an important class of steels that are similar to plain carbon steels, but they typically contain small amounts of strong carbide forming elements such as niobium, vanadium and

DISCLAIMER

titanium. The carbide formers serve to add precipitation strengthening, grain refinement and control over the transformation temperatures, while adding minimal additional raw material cost. Depending on the processing route, these steels have microstructures that are similar to the plain carbon steels (e.g. ferrite-pearlite). Given the similarity, the purpose of the present work was to evaluate the extent to which austenitization models developed for plain carbon steels are applicable to the microalloyed steels. Applying the low carbon steel model to the transformation kinetics of Timken 1054V1 seamless steel tubing will be the focus of this paper. Timken 1054V1 alloy is an experimental composition being developed for various applications requiring a surface hardness of 60 HRC. Of particular interest is examining both as-pierced and normalized tubing. The two conditions were made from the same heat and therefore have the same composition, but the microstructures vary significantly in terms of pearlite volume fractions, prior austenite grain sizes, and potentially, microalloy carbide distributions.

EXPERIMENTAL

Materials and Processing

The heat of microalloyed 1054V1 used in this study was melted from scrap iron in a 150 ton electric furnace, ladle refined and strand cast into 28 cm by 37.5 cm blooms. The blooms were then reheated and rolled to an 20.3 cm diameter round bar, reheated to around 1230°C and pierced into a 17.8 cm OD by 1.9 cm wall tube, followed by air cooling on a hot bed. Part of the tubing was subsequently production normalized by reheating to 900°C followed by air cooling. The chemistry of the final product can be found in Table I. Samples from both the hot rolled (as-pierced) and the normalized tubing were then sectioned to remove 6.35 mm diameter by 127 mm long dilatometry specimens. The mechanical properties of the tubing in both conditions can be found in Table II.

The microstructure of the hot rolled tubing is composed of coarse grained pearlite with proeutectoid ferrite at the prior austenite grain boundaries, Figure 1(a). The normalized tubing is composed of fine grained pearlite with ferrite at the prior austenite grain boundaries, Figure 1(b). The relevant grain size and constituent volume fraction measurements can be found in Table III, and it is important to note the significant differences in the relative fractions of the constituents.

Dilatometry

To characterize the phase transformations, dilatometry experiments were performed using a DSI Gleeble 1500 thermomechanical simulator. A high resolution dilatometer was used to measure the diametral dilatation of solid 6.35 mm diameter

Table I Steel chemistry of 1054V1 material used in this study.

Element	C	Mn	P	S	Si	Cr	Ni	Mo	Cu	Al	V	N
Percent	0.55	0.78	0.01	0.032	0.24	0.14	0.09	0.02	0.17	0.02	0.10	0.012

Table II Mechanical properties of 1054V1 material.

Condition	Hardness		Tensile Strength	Yield Strength	Percent Elong.	Percent RA	CVN Impact
	BHN	HRC	MPa	MPa			Joules
Hot Rolled	275	25	917	555	14.5	35	11.5
Normalized	240	19	820	510	20	47	20

Table III Microstructural properties of 1054V1 material.

Condition	Prior Austenite Grain Size ASTM (μm)	Ferrite (Percent)	Pearlite (Percent)	Ferrite Grain Size ASTM (μm)
Hot Rolled	3.25 (116)	9.5	90.5	11 (8)
Normalized	7.5 (25)	28.4	71.6	11 (8)

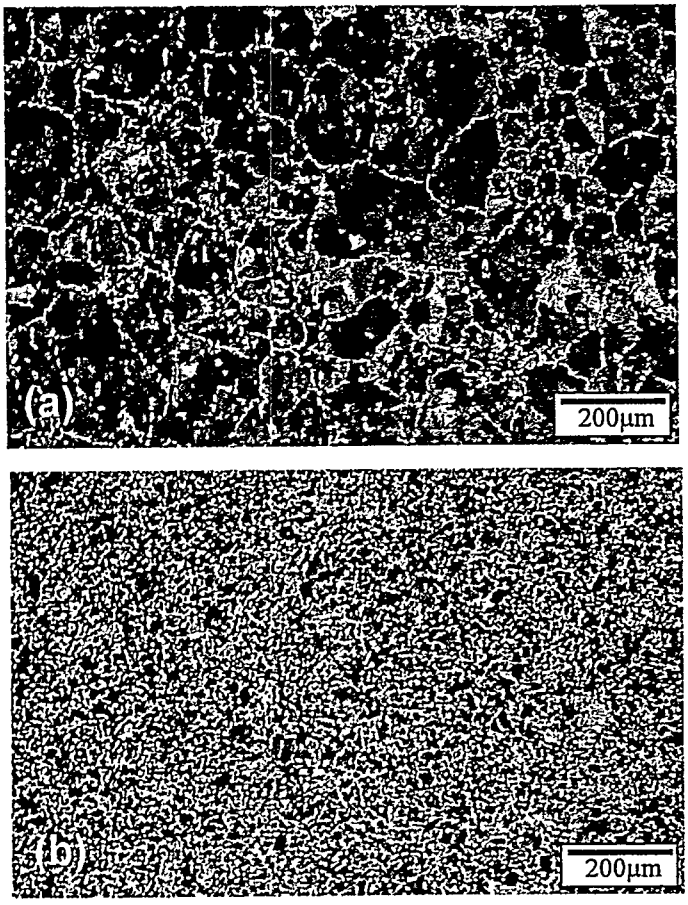

Figure 1. Photomicrographs of Timken alloy 1054V1 initial microstructures. The hot rolled (as-pierced) microstructure (a) contains a coarse grain ferrite with proeutectoid ferrite at the prior austenite grain boundaries while the production normalized condition (b) contains a much finer grained pearlite with significantly more proeutectoid ferrite present.

specimens using the low stress modified dilatometry technique.[15] Specimens in the hot rolled and normalized conditions were heated with linearly programmed temperature ramp rates from 50°C/s to 500°C/s to simulate the heating rates that occur during rapid thermal cycle processes. The rapidly quenched specimens were tubular with a 6.35 mm outer diameter and a 4.55 mm inner diameter that was internally quenched from the peak temperature with helium gas. This produced a cooling rate of approximately 250°C/s between 800°C and 500°C. All tests were conducted in an argon atmosphere.

Model

A model was previously developed that relates the on-heating phase transformations to

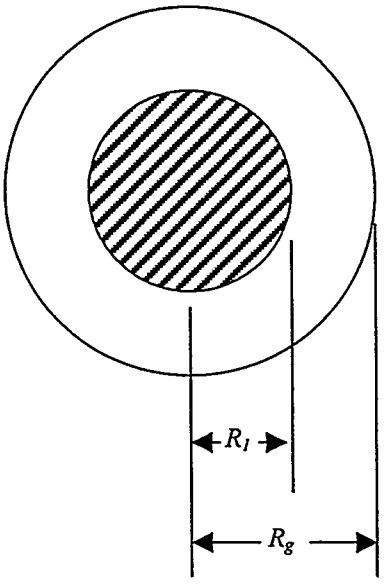

Figure 2. Idealized initial microstructure consisting of a spherical pearlite nodule of radius R_l surrounded by a shell of ferrite of radius R_g.

volume changes that are measured by dilatometry. The main features of the model are presented below and additional detail can be found in the work by Dykhuizen et al.[14]

The model begins by assuming a single representative grain that is spherical in geometry and contains a pearlite colony within a shell of ferrite, see Figure 2. The grain size is represented by the prior austenite grain size, R_g which is one of the required inputs to the model. Another required input for the model is the volume fraction of pearlite, F_p, which is experimentally determined from micrographs. The average size of the pearlite region within a grain, R_l is calculated by:

$$R_l = R_g (F_p)^{\frac{1}{3}} \qquad (1)$$

As the steel is heated above the A_{c1} temperature, the pearlite is assumed to transform to austenite based on Avrami kinetics.[16] The governing equations for the reactions are as follow:

$$\frac{dA}{dt} = (A_{\max}(T) - A) n K(T) \theta^{(n-1)} \qquad (2)$$

where

$$\theta = \left[\frac{-\ln\left(\frac{A_{\max}(T) - A}{A_{\max}(T)} \right)}{K(T)} \right]^{\frac{1}{n}} \quad (3)$$

and

$$K(T) = \exp\left(\alpha - \frac{\beta}{T} \right) \quad (4)$$

where A is the fraction of pearlite transformed and A_{max} as the maximum amount of pearlite that can transform to austenite as a function of temperature. In practice, A_{max} is a step function that equals 100% above A_{e1} and 0% below. The reaction order, n, is assumed to be three based on previous work performed by Speich and Szirmae.[3] The θ term, a fictitious time, is set equal to the time that is required to obtain the current extent of reaction at the current temperature. The K(T) term is a temperature-dependent rate parameter that in theory could be determined from a time temperature transformation (TTT) curve for eutectoid pearlite. To eliminate the need for a detailed TTT curve for each alloy, a functional form that is consistent with Speich and Szirmae[3] is assumed and fit with experimental data which provides two of the fitting parameters that are used in this model, α and β.

A separate diffusion-limited model is used for the surrounding ferrite shell, a modeling approach that is similar to that used by other researchers.[17]

$$\frac{dr}{dt} = \left(\frac{\gamma D(T) \frac{\Delta c}{\Delta x}}{c_i(T) - c_{fo}} \right) \left(\frac{R_{\max}(T) - r}{R_b - R_1} \right) \quad (5)$$

The radial location of the boundary between the untransformed ferrite and the austenite is denoted by r. The term r can range from R_1 to R_{max}. The term R_{max} is calculated to assure that the carbon content of the resulting austenite is not below the A_{c3} line. The left hand terms represent the carbon concentrations with c_{fo} being the initial carbon concentration of the ferrite, c_i(T) is the austenite carbon concentration at the interface, and $\Delta c / \Delta x$ is the carbon concentration gradient at the ferrite/austenite interface. The diffusion coefficient of carbon in austenite is D(T)[18]. A fitting term, γ is the final parameter in the above expression. Essentially γ is used to compensate for the differences in the actual prior austenite grain shape and the assumed spherical shape, as well as the assumed simplifications of carbon diffusion in austenite.

While the fundamental principals of the Dykhuizen et al.[14] model, summarized above, were used in this study, several changes to the model were necessary to simulate the microalloyed steels. The amount of pearlite that forms in a steel is sensitive to the cooling rate of the austenite. In particular, rapid cooling of austenite can result in a larger than predicted equilibrium volume fraction of pearlite. The non-equilibrium value of pearlite has a carbon content that is lower than the eutectoid composition. In this study, the effect of cooling rate was readily seen as the hot rolled samples had greater than 90 vol% of pearlite compared with the normalized that had 71 vol% of pearlite. Therefore, to properly simulate non-equilibrium pearlite volume fraction steels, it was necessary to modify the model.

The calculation of the carbon content of the austenite that was created from the pearlite colonies was modified to account for the non-equilibrium volume fractions. When the temperature rises above the A_{e1} line, austenite is created at the eutectoid carbon content. To accomplish this, cementite and ferrite are transformed to austenite in proportions that leave the untransformed pearlite with excess ferrite. As the temperature rises, the carbon content of the austenite reduces as described by the A_{e3} line. The austenite carbon content continues reducing until it reaches the average carbon content of the pearlite colonies. Then, the carbon content of the austenite created from the pearlite remains constant at this value.

In the new model, the state variable A now represents the fraction of cementite within the pearlite colonies that has transformed to austenite, not the fraction of pearlite (although in practice these two quantities are nearly equal). The volume fraction of ferrite in the pearlite colonies that has transformed to austenite is then determined from the austenite carbon content as described above. Finally, the proeutectoid ferrite is not allowed to transform until the austenite carbon content has reduced to the pearlite carbon content eliminating the possibility of creating austenite at carbon contents lower than specified by the A_{e3} line.

RESULTS AND DISCUSSION

Samples were tested using high resolution Gleeble dilatometry as described above. A typical dilatation curve for the formation of austenite in a hypoeutectoid steel is shown in Figure 3. As the specimen is heated at a constant rate from room temperature, the thermal expansion of the material is the dominant feature causing the diameter to increase with a nearly constant positive slope. However, at approximately 735°C the pearlite begins to form austenite as the A_{c1} temperature is reached. The sharp contraction (vertical drop) in the data is associated with the formation of austenite from the pearlite. The formation of austenite then continues as the proeuctectiod ferrite reacts to form austenite, albeit at a much slower rate, with the reaction continuing to approximately 860°C at which point the A_{c3} temperature is reached. The completion of the austenite formation is observed in the data, as the expansion of the material becomes linear above approximately 860°C with a slope that is steeper than that seen in the original ferrite-pearlite specimen. The above interpretation of the dilatation curve is somewhat simplified as there is actually a point where the pearlite is forming austenite at the same time as the proeutectoid ferrite. Detailed analysis of the curves was performed using the model presented previously, as it is necessary to use the model to accurately analyze the curve.[14]

The solid specimens were first tested using Gleeble dilatometry and the results examined using

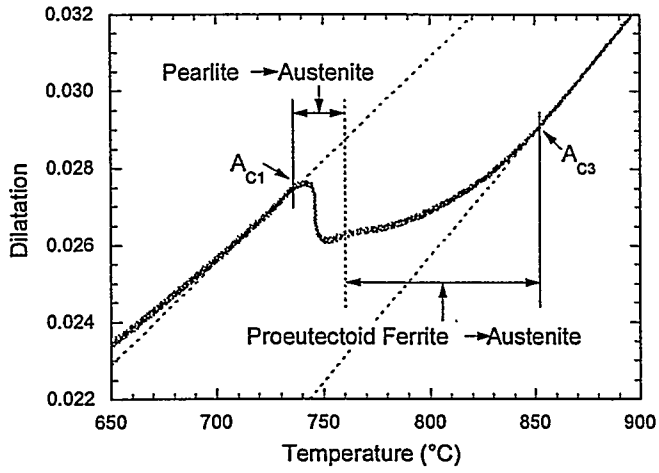

Figure 3 Typical dilatometry curve obtained from a hypoeutectoid steel heated at a constant rate. The pearlite in the specimen begins to form austenite once the A_{c1} temperature is reached. The pearlite completes reacting quickly, and the proeutectoid ferrite then begins to form austenite at a much slower rate. The formation of austenite is complete once the A_{c3} temperature is reached.

the austenitization model. The various samples all had the same chemistry, but two different prior austenite grain sizes and volume fractions of pearlite. Analysis of a series of three dilatometry curves (at 50, 100, and 200°C/sec) for the normalized material yielded fitting parameters of $\alpha = 232$, $\beta = 236000$, and $\gamma = 1.93$. The experimental curves and model fits are shown in Figure 4(a) for $\Delta L/L$ versus time and for $\Delta L/L$ versus temperature. The model fits are very good for the normalized data, implying that the model assumptions are reasonable for the 1054V1 normalized material.

Figure 5 shows the fraction austenite as a function of temperature for the normalized material heated at 100°C/sec, and shows the relative contributions from the pearlite and ferrite constituents. Figure 5 illustrates the rapid decomposition of the pearlite that is associated with the short diffusion distance (approximately half the pearlite interlamella spacing). The longer tail associated with the completion of the transformation of the ferritic regions is more gradual since the temperature has to traverse the two phase region between the A_{c1} and aA_{c3} lines.

Because three fitting parameters are used in the model, a good fit to one set of dilatation curves

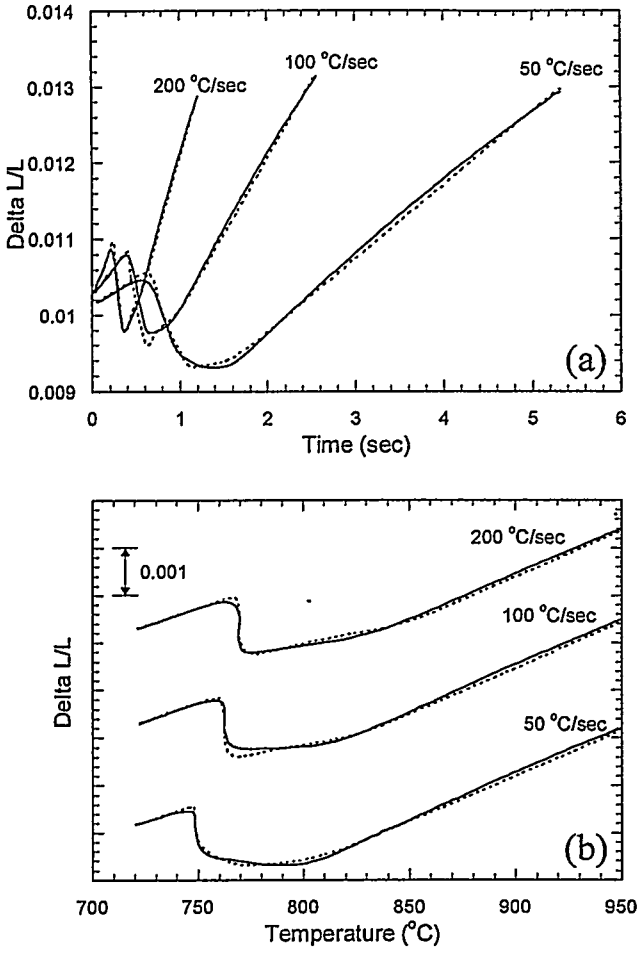

Figure 4. Comparison of normalized experimental dilatation data (solid) to model predictions (dashed) for three different heating rates: (a) time dependence and (b) temperature dependence. For clarity, the temperature dependent curves are displaced in ΔL/L.

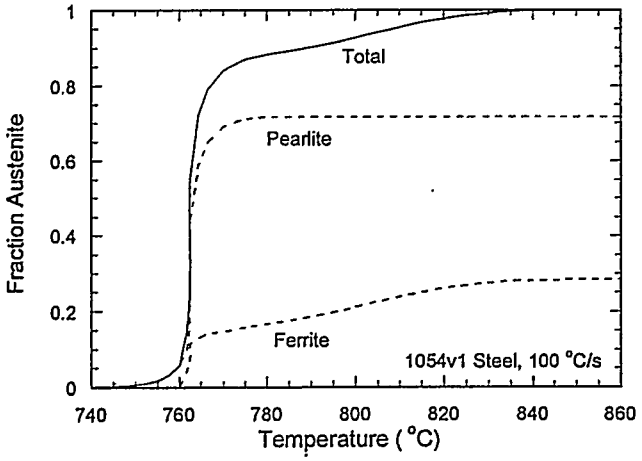

Figure 5. Volume fraction of austenite formed as a function of temperature for the normalized material heated at the 100°C/s heating rate. The relative contributions from the initial ferrite and pearlite phases are also shown as predicted by the model.

is not necessarily indicative of its general applicability. Additional experimental trials were therefore conducted at heating rates both within and outside of the range used to develop the parameter set. The data from these trials was then compared with calculated results obtained by using the parameters developed from the initial experiments. The results of these comparisons are shown in Figure 6, and the calculated curves are in good agreement with the experimental data. Thus, the fitting parameters obtained with one set of data worked quite well with other sets of data for heating rates within the initial range, and extrapolated reasonably to a heating rate of 500°C/s. Using the parameters for one set of data to accurately predict another set of data confirms the experimental repeatability and suitability of the parameter set for the normalized material. The prediction for the

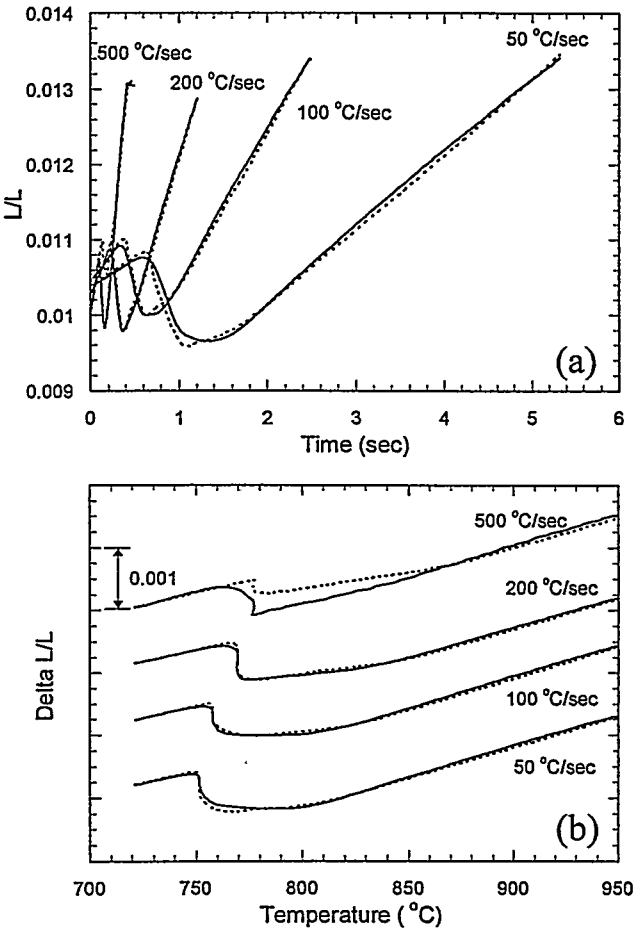

Figure 6. Comparison of experimental dilatation data (solid) to model predictions (dashed) for a different series of three normalized tests.: (a) time dependence and (b) temperature dependence. The plots show very good model prediction for the set of new specimens. For clarity, the temperature dependent curves are displaced in ΔL/L.

500°C/s transient, though quite reasonable considering the rapid cycle, is not as well predicted as the other transients. The reasons for this reduced accuracy are not fully clear, but may be related to the mobility of the alloy elements in the microalloyed steel. As discussed below, the effect of these elements is not explicitly described in the current model, but may affect the kinetics though their slower (than carbon) diffusion rates and partitioning to the various phases.

The fit of the normalized 1054V1 data yielded parameters that are similar to those obtained in the original study of 1026 steel[14] (α = 201, β = 200000,and γ = 2.23). This implies that the transformation mechanisms are similar for the two steels (and their respective starting microstructures). It is interesting to compare predictions for the 1054V1 steel based on the parameter set developed for the 1026 steel. Figure 7 shows these predictions and indicates that though the predictions are reasonable, they are less accurate than the fits obtained using the 1054V1 parameters as shown in Figure 3. Stated differently, the curves of Figure 7 illustrate the expected transformation behavior for 1026 steel given the same thermal cycle as the 1054V1 steel. For the three heating rates, the 1026 parameters generally predicted a faster reaction, Figure 7(a), at lower start temperatures, Figure 7(b) for the formation of austenite than what is experimentally observed in the 1054V1. Although these figures are complex and difficult to interpret directly because of the thermal arrest during the transformation,[14,19] it is reasonable to conclude that the austenite formation kinetics of the 1054V1 are retarded relative to the 1026 steel. There are several possible sources for the differences in the kinetics. First, the current model does not explicitly include pearlite spacing. Differences in the pearlite spacing between the original 1026 and the normalized 1054V1 could affect the dissolution rate of the pearlite. In addition, it is also likely that differences in the kinetics can be attributed to the microalloy additions. With respect to the pearlite decomposition, partitioning of the carbide forming elements to the carbide within the pearlite might be expected to kinetically retard decomposition of the pearlitic carbide. Moreover, the alloying elements would be expected to influence the diffusion rate of

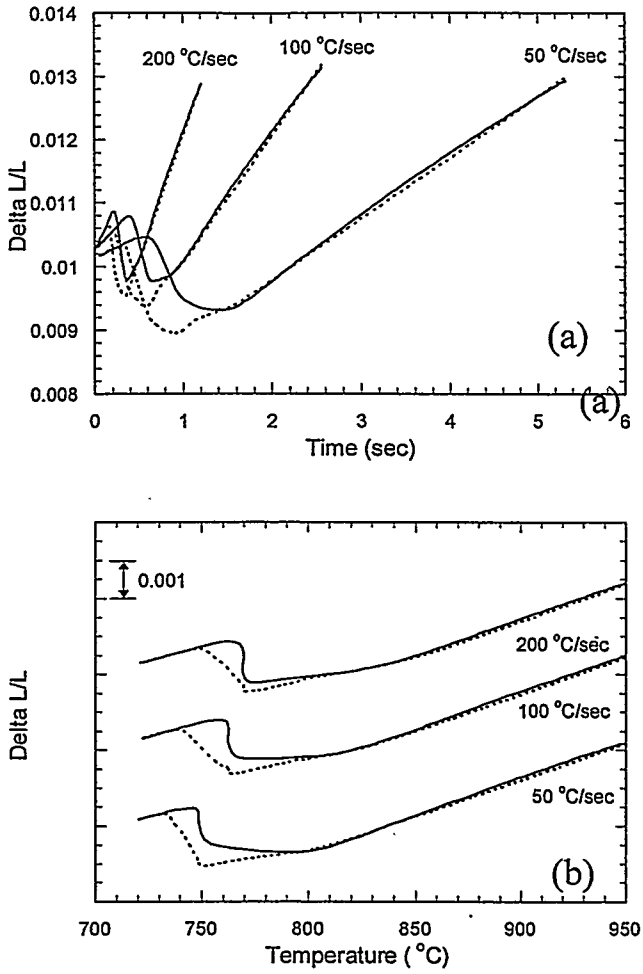

Figure 7. Comparison of normalized experimental dilatation data (solid) to model predictions (dashed), where the parameters from the original study of 1026 data were used: (a) time dependence and (b) temperature dependence. The 1026 parameters generally show a more rapid rate and lower transformation start temperatures for the 1026 parameter model predictions. For clarity, the temperature dependent curves are displaced in $\Delta L/L$.

carbon, thereby affecting the dissolution of the pearlite as well as the dissolution of the proeutectoid ferrite.

Model fits for microalloyed 1054V1 hot rolled steel are shown in Figure 8. The model gives reasonable representation of the data, and the fit parameters for this condition were found to be α = 378, β = 392000, and γ = 0.59. Due to the low fraction of ferrite in the hot rolled condition, Table III, the γ parameter has little impact on the model

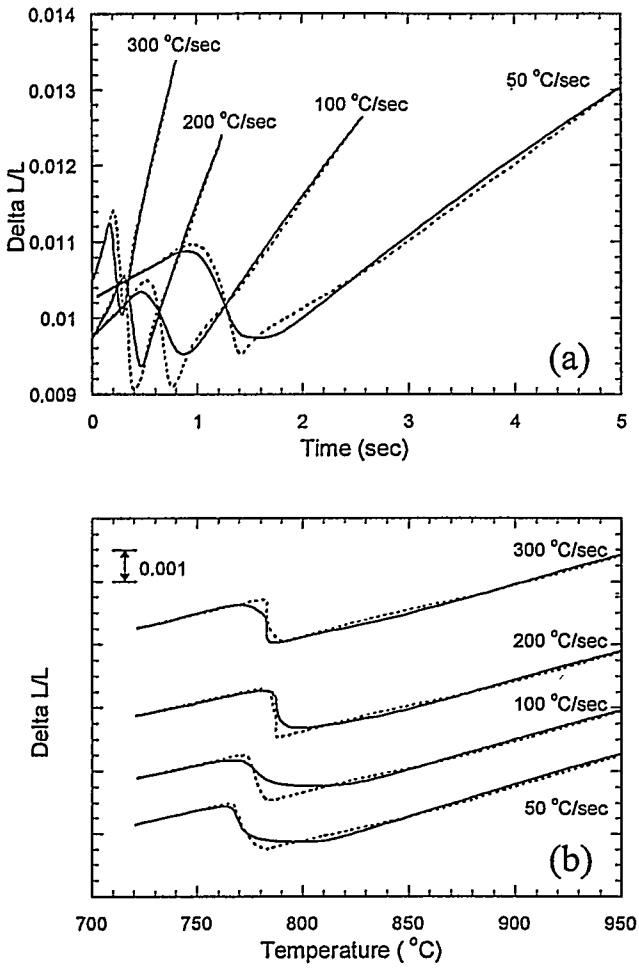

Figure 8. Comparison of hot rolled experimental dilatation data (solid) to model predictions (dashed) for three different heating rates: (a) time dependence and (b) temperature dependence. For clarity, the temperature dependent curves are displaced in ΔL/L.

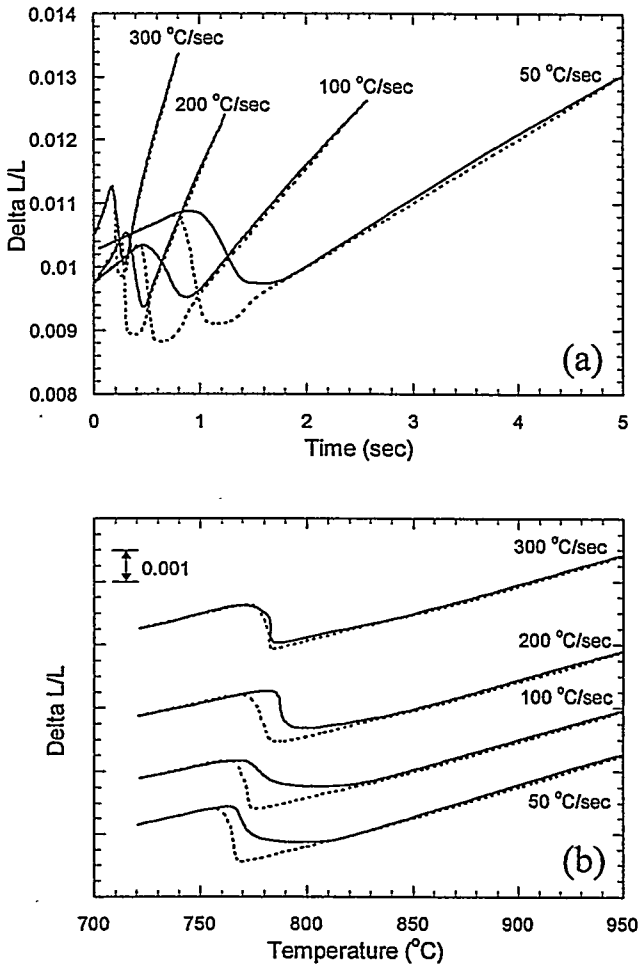

Figure 9. Comparison of normalized parameters used to predict (dashed) the experimental hot rolled dilatation data (solid): (a) time dependence and (b) temperature dependence. The fit is very inaccurate with the actual austenite formation occurring much slower in the hot rolled material than is predicted with the normalized parameters. For clarity, the temperature dependent curves are displaced in ΔL/L.

and can vary appreciably from 0.59 without significantly altering the results. However, even neglecting the third parameter, the first two parameters are also significantly different than those obtained from the normalized material. This can be illustrated by using the normalized parameter set to predict the hot rolled response. The comparison shown in Figure 9 was accomplished by inputting the correct hot rolled grain size and pearlite fraction and using the normalized kinetic parameters of α = 232, β = 236000, and γ = 1.93. The fit in Figure 9 is quite inaccurate, with the actual austenite formation occurring much slower in the hot rolled material than is predicted by the model for the normalized material. For the two microstructural starting conditions, the major differences are in the fraction pearlite and grain size (although there may also be fine scale differences in terms of microalloy carbides). For the hot rolled material, the fraction of pearlite is significantly different than would be expected at equilibrium. However, the current model accounts for this discrepancy as described in the modeling section. The formation of non-equilibrium pearlite fractions occurs when the material is transformed to pearlite and ferrite at temperatures significantly below the equilibrium

transformation temperature (as in the hot rolled material). This has the effect of altering both the pearlite spacing and the relative thickness of the carbide and ferrite lamella within the pearlite. The current model does not capture these differences explicitly, but they are captured indirectly in the parameters associated with the pearlite decomposition. Therefore, it is perhaps not surprising that different fit parameters were obtained for the two starting microstructures.

The above comparisons reinforce the introductory comments regarding the relative complexity of austenite formation in steels, and demonstrates the sensitivity of the process to the starting microstructure. They also illustrate the potential difficulties associated with development of a general model for the on-heating transformations, since such a model must account either explicitly or implicitly (as in the current model) for the details and range of starting microstructures. Moreover, it was generally observed that the austenite formation was experimentally more repeatable in the normalized material than in the hot rolled. This difference is consistent with typical shop floor experience, that more repeatable results are obtained from normalized material during rapid thermal cycle processes.

Direct verification of an on-heating model during a rapid thermal cycle is extremely difficult. Techniques such as hot stage microscopy are needed to directly view the formation of austenite since austenite transforms to other phases when cooled. Unfortunately, heating rates in this study are orders of magnitude faster than that available with hot stage microscopy. Another complicating factor is the very short time required for the reaction to complete; at most two seconds in the current range of heating rates. Thus, indirect methods to validate the model are required. In this study, experiments were performed on tubular specimens that were partially austenitized. A 1054V1 normalized tubular specimen was heated at a linearly programmed rate of 50°C/s to a fixed temperature of 785°C. The specimen was immediately quenched internally with helium gas to room temperature in an effort to transform as much of the austenite to martensite as possible. The quench rate was approximately 250°C/s between 800°C and 500°C. Figure 10 shows the thermal cycle and measured dilatation for the specimen. The actual temperature cycle displays the typical deviation from a linear ramp around 720 °C. The deviation is due to the endothermic reaction of pearlite transforming to austenite. The Gleeble 1500 control algorithm attempts to, but does not totally, eliminate the arrest.[19]

After quenching, the tubular specimen was sectioned and etched in a 2% nital solution for microstructural examination. Optical microscopy was performed to examine the amount of remaining ferrite. Figure 11 is an oil immersion image that

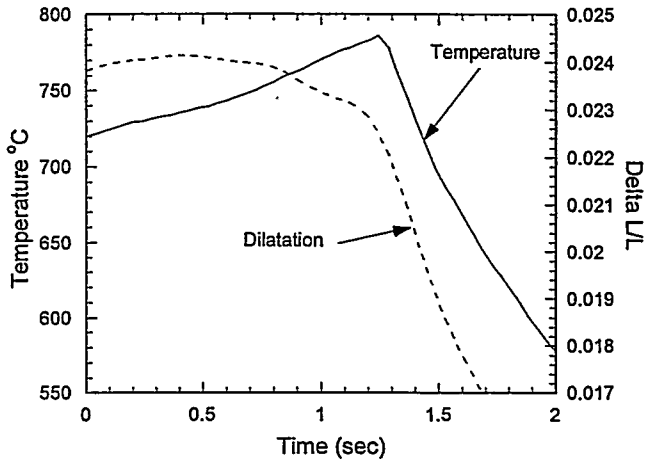

Figure 10. Measured thermal cycle (solid) and dilatation data (dashed) for a hollow normalized specimen heated to 785°C and quenched internally with helium gas.

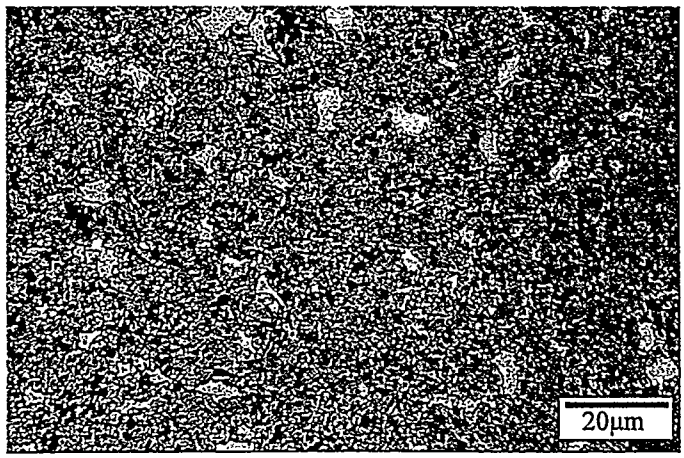

Figure 11. Optical micrograph after quenching of the normalized tubular specimen.

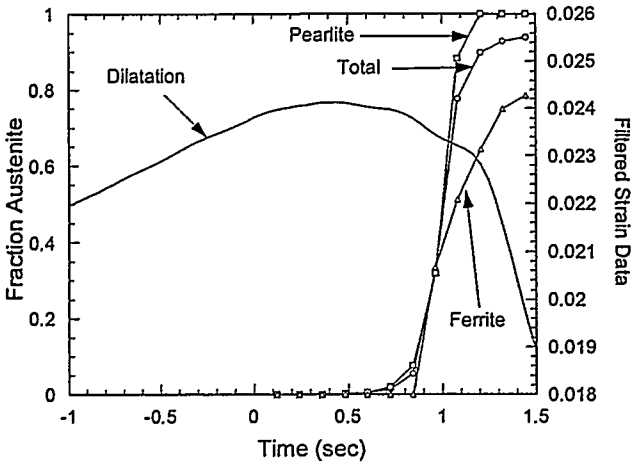

Figure 12 Predicted fraction transformed and measured dilatation as a function of time for the normalized tubular quenched specimen.

shows a typical cross section of the partially transformed specimen. Blocky white areas of undisolved ferrite can be seen in the structure. In addition, the structure appears to be a mixture of martensite, gray regions, and upper transformation products (bainite or very fine new pearlite), dark regions. Quantitative image analysis of several micrographs was attempted, but it was difficult to isolate the ferrite and produced somewhat unpredictable results. However, point count results of 20 fields, 50 counts per field, resulted in an average of 6.05% ferrite.

The actual temperature transient of the tubular specimen was used as input for the model. Predictions of the fractions of pearlite and proeutectoid ferrite transformed to austenite were then calculated. The predictions as a function of time are plotted in Figure 12, along with the actual dilatometer data from the experiment. Figure 12 shows that all of the pearlite is predicted to transform to austenite. However, the amount of ferrite predicted to transform is only 78.3%. Therefore, the final volume of ferrite predicted is 78.3% of the amount of ferrite initially present, which was 28.4% of the total volume. Thus the total remaining volume fraction of ferrite is predicted to be 6.2%, a value very close to the measured value of 6.05%.

CONCLUSIONS

The model parameters for the normalized 1054V1 material were compared to parameters previously generated for 1026 steel, and the transformation behavior was relatively consistent. Validation of the model predictions by heating into the austenite plus undisolved ferrite phase field and rapidly quenching resulted in reasonable predictions when compared to the measured volume fractions from optical metallography. The hot rolled 1054V1 material, which had a much coarser grain size and a non-equilibrium volume fraction of pearlite, had significantly different model parameters and the on heating transformation behavior of this material was less predictable with the established model. The differences in behavior is consistent with conventional wisdom that normalized micro-structures produce a more consistent response to processing, and it reinforces the need for additional work in this area.

ACKNOWLEDGEMENTS:

Sandia is a multiprogram laboratory operated by Sandia Corporation, a Lockheed Martin Company, for the United States Department of Energy under Contract DE-AC04-94AL85000

REFERENCES

1. G. A. Roberts and R. F. Mehl, The Mechanism and the Rate of Formation of Austenite from Ferrite-Cementite Aggregates, Trans. ASM, Vol. 31, pp. 613-650, (1943).

2. E. S. Davenport and E. C. Bain, Trans AIME, Vol. 90, pp. 117-131, (1930).

3. G. R. Speich and A. Szirmae, Formation of Austenite from Ferrite and Ferrite-Carbide Aggregates, Trans. AIME, Vol. 245, pp. 1063-1069, (1969).

4. G. Molinder, A Quantitative Study of the Formation of Austenite and the Solution of Cementite at Different Austenitizing Temperatures for a 1.27% Carbon Steel, Acta Metall., Vol. 4, pp. 565-571, (1956).

5. R. R. Judd and H. W. Paxton, Kinetics of Austenite Formation from a Spheroidized Ferrite-Carbide Aggregate, Trans. AIME, Vol. 242, pp. 206-215, (1968).

6. C. I. Garcia and A. J. DeArdo, Formation of Austenite in 1.5 Pct Mn Steels, Met. Trans.A, Vol. 12A, pp. 521-530, (1981).

7. P. A. Wycliffe, G. R. Purdy, and J. D. Embury, Growth of Austenite in the Intercritical Annealing of Fe-C-Mn Dual Phase Steels, Canadian Metallurgical Quarterly, Vol. 20, pp. 339-350, (1981).

8. D. F. Watt, L. Coon, M. Bibby, J. Goldak, and C. Henwood, An Algorithm for Modeling Microstructural Development in Weld Heat-Affected Zones (Part A) Reaction Kinetics, Acta Metall., Vol. 36, No. 11, pp. 3029-3035, (1988).

9. T. Akbay, R. C. Reed, and C. Atkinson, Modeling Reaustenitisation from Ferrite/Cementite Mixtures in Fe-C Steels, Acta Metall. Mater., Vol. 47, pp. 1469-1480, (1994).

10. C. Atkinson, T. Akbay, and R. C. Reed, Theory for Reaustenitisation from Ferrite/Cementite Mixtures in Fe-C-X Steels, Acta Metall. Mater., Vol. 43, pp. 2013-2031, (1995).

11. C. Atkinson and T. Akbay, The Effect of the Concentration-Dependent Diffusivity of Carbon in Austenite on a Model of Reaustenitisation from Ferrite/Cementite Mixtures in Fe-C Steels, Acta Mater., Vol. 44, pp. 2861-2868, (1996).

12. T. Akbay and C. Atkinson, The Influence of Diffusion of Carbon in Ferrite as well as Austenite on a Model of Reaustenitization from Ferrite/Cementite Mixtures in Fe-C Steels, J. Materials Science, Vol. 31, pp. 2221-2226, (1996).

13. L. Gavard, H. K. D. H. Bhadeshia, D. J. C. MacKay, and S. Suzuki, Bayesian Neural Network Model for Austenite Formation in Steels, Materials Science and Technology, Vol. 12, pp. 453-463, (1996).

14. R. C. Dykhuizen, C. V. Robino, and G. A. Knorovsky, A Method for Extracting Phase Change Kinetics from Dilatation for Multistep Transformations: Austenitization of a Low Carbon Steel, Metallurgical and Materials Transactions B, Vol. 30B, pp. 107-117, (1999)

15. J. D. Puskar, manuscript in preparation.

16. J. W. Christian: *The Theory of Phase Transformations in Metals and Alloys, Part I*, Pergamon Press, New Your, NY, 1981 pp. 525-48

17. A. S. Oddy, J. M. J. McDill, and L. Karlsson, Microstructural Predictions Including Arbitrary Thermal Histories, Reaustenization and Carbon Segregation Effects, Can. Met. Quarter., Vol. 35, pp. 275-283, (1996).

18. E. A. Brandes, *Smithells Metals Reference Book Sixth Ed.* , Butterworths, London, p. 13-58, (1983).

19. C. V. Robino, G. A. Knorovsky, R. C. Dykhuizen, D. Q. MacCallum, and B. K. Damkroger, Transformation Kinetics in Controlled-Power and Controlled-Temperature Cycle Testing, Accepted for Publication in Proceedings of the 5th International Conference on Trends in Welding Research, S. A. David, ed., Pine Mountain, GA, (1998).

For further information on this paper, please contact Joseph D. Puskar at Sandia National Laboratories, PO Box 5800, MS 0367, Albuquerque, NM 87123-0367 or jdpuska@sandia.gov